Peer-reviewed version available at *Appl. Sci.* **2020**, *10*, 2146; doi:10.3390/app10062146

Article

Open-Circuit Fault Diagnosis of Wind Power Converter Using Variational Mode Decomposition, Trend Feature Analysis and Deep Belief Network

Jingxuan Zhang [1,2], Hexu Sun [1,3,*], Zexian Sun [2], Yan Dong [1] and Weichao Dong [1,3]

[1] School of Artificial Intelligence, Hebei University of Technology, Tianjin 300130, China; jingxuan.zhang@ncst.edu.cn (J.Z.); dongyan73@hebut.edu.cn (Y.D.); dongweichao@hebust.edu.cn (W.D.)
[2] College of Electrical Engineering, North China University of Science and Technology, Tangshan 063210, China; sunzx@ncst.edu.cn
[3] School of Electrical Engineering, Hebei University of Science and Technology, Shijiazhuang 050018, China
* Correspondence: hxsun@hebust.edu.cn; Tel.: +86-1503-398-1253

Abstract: The power converter is the significant device in a wind power system. Wind turbine will be shut down and off grid immediately with the occurrence of the IGBT module open-circuit fault of power converter, which will seriously impact the stability of grid and even threaten personal safety. However, in the existing diagnosis strategies of power converter, there are few single and double IGBT modules open-circuit fault diagnosis methods producing negative results including erroneous judgment, omissive judgment and low accuracy. In this paper, a novel method to diagnose the single and double IGBT modules open-circuit faults of the permanent magnet synchronous generator (PMSG) wind turbine grid-side converter (GSC) is proposed. Above all, collecting the three-phase current varying with wind speed of 22 failure states including a normal state of PMSG wind turbine GSC as the original signal data. Afterward, the original signal data are decomposed by using variational mode decomposition (VMD) to obtain the mode coefficient series, which are analyzed by the proposed method base on fault trend feature for extracting the trend feature vectors. Finally, the trend feature vectors are used as the input of deep belief network (DBN) for decision-making and obtaining the classification results. The simulation and experimental results show that the proposed method can diagnose the single and double IGBT modules open-circuit faults of GSC, and the accuracy is higher than the benchmark models.

Keywords: power converter; fault diagnosis; intelligent algorithm; variational mode decomposition; deep belief network

1. Introduction

The capacity of power converter in recent years has steadily grown in step with increased size of large wind turbines, correspondingly, the load capacity of components of converter improved evidently and the electrical structure is more complex, which is bound to raise the failure rate greatly [1,2]. Meanwhile, the wind farms are mostly built in areas with abundant wind resources and complex weather climate [3,4]. The operational ambient of power converter is extremely harsh, and the failure rate is high [5]. The core device of the power converter of wind turbine is the power switching component--insulated gate bipolar transistor (IGBT) module [6]. A lot of harmonics and interharmonics will be produced if the IGBT module in a power converter has short-circuit or open-circuit, which will impact the power quality and pollute the grid. Then the wind turbine would be shut down and off grid immediately, so as not to seriously impact the stability of grid and even threaten personal safety [7]. The existing researches are matured for the short-circuit fault of power converter, and there are corresponding modules for protection. Though a few achievements for the IGBT module open-circuit fault of power converter over the years, there are few single and double IGBT modules open-circuit fault diagnosis methods producing negative results including erroneous

judgment, omissive judgment and low accuracy. Moreover, due to the capability of the protection module, the short-circuit fault will turn into an open-circuit fault. Therefore, the open-circuit fault diagnosis of wind turbine power converter is crucially significant, whose essence is to diagnose power switching component, such as IGBT module.

Over the past decade, a number of studies have been made concerning open-circuit fault diagnosis of IGBT module in power converter [8-13], which can be divided into qualitative fault diagnosis and quantitative fault diagnosis. Qualitative fault diagnosis includes fault tree analysis method and expert system method, whose basic idea is to build a knowledge base by using the effective experience and expertise accumulated by experts in the case of open-circuit fault of power converter, and to determine the diagnosis results and fault causes according to certain logic reasoning for the fault status. Quantitative fault diagnosis includes current detection method and voltage detection method, which analyze and compare the current, voltage and other operating electrical parameters of power converter, set thresholds when necessary, so as to make decision and classification. The method of qualitative fault diagnosis is intuitionistic and easy to understand with clear thinking and strong logic. However, with the increasing complexity of power converter system, the knowledge base is not comprehensive enough and the logic reasoning process is extremely complex, which makes the process of diagnosis and search difficult and the accuracy of fault diagnosis low. In order to improve the efficiency and accuracy of fault diagnosis, a combination of qualitative fault diagnosis and quantitative fault diagnosis is usually used. As stated in [14], the zero current periods are registered in each converter phase circuits. The open-circuit faults are identified calculating the average values of differences between predicted and measured phase currents. This method is insensitive to load changes but out of the high power application. [15] proposes an approach, which is based on the absolute normalized Park's current vector. This method can detect multiple open-circuit switch faults. But, this method is also prone to false alarm or failure alarm when the load changes abruptly. In [16], wavelet transform is used to preprocess load current signals, and open-circuit faults are diagnosed by the processed currents based on BPNN and CART. As stated in [17], the fault diagnosis strategy utilizes the average values of the voltage to quickly identify failures position and devices. But the direction of the inductor current on the primary side has to be considered first of all.

The rest of this paper is organized as follows. In Section 2, the focused topology of GSC of PMSG wind turbine and IGBT modules open-circuit faults are addressed and analyzed. Afterward, The mathematical models of VMD, trend feature analysis method and DBN model are established and described in Section 3, respectively. Section 4 and 5 deals with the analytical calculation of numerical simuation and experiment, some comparison results of fault diagnosis methods are shown in the end of the sections. The concluding remarks are drawn in Section 6.

2. Topological Graph and Fault Analysis

Up to now, the doubly fed induction generator (DFIG) and PMSG wind turbines equipped partial scale and full scale power converters, respectively, have occupied the majority of the wind power market [18,19]. Initially, the DFIG became attractive due to the controllability of active and reactive power, having the mature technology and low cost. However, grid code has regularly updated, and become stricter and stricter with the steady increase of wind power penetration. Therefore, more and more wind farm operators turn to using the PMSG wind turbine equipped full scale power converter, due to the better low-voltage ride-through capability, higher efficiency and power density [20,21].

2.1. GSC Modeling

Although various power switching components can be used to match a full scale power converter, this paper only focuses on the GSC with the back to back dual pulse width modulation (PWM) structure, as it is the most used structure in the wind turbine industry. Figure 1 shows the topological graph of the GSC.

Preprints (www.preprints.org) | NOT PEER-REVIEWED | Posted: 26 February 2020 doi:10.20944/preprints202002.0392.v1

Peer-reviewed version available at Appl. Sci. 2020, 10, 2146; doi:10.3390/app10062146

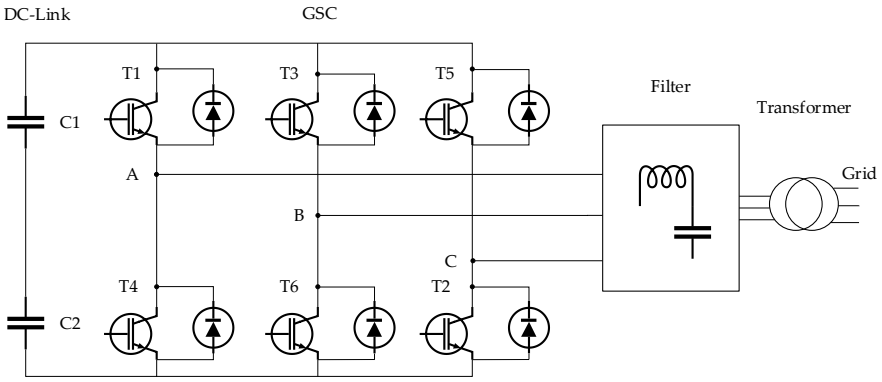

Figure 1. The topological graph of the GSC.

In the Figure 1, DC-Link is mainly consisted of shunt capacitors (C1 and C2), whose two-terminal provides a stable direct current (DC) voltage to GSC. The GSC is mainly composed of 6 IGBT modules. Every two IGBT modules compose phase A, B and C, respectively. Through PWM control strategy, the DC voltage is transformed into sinusoidal alternating current with required equivalent frequency and amplitude. Afterward, the harmonic and peak are suppressed and filtered by the filter, and the power is fed to the grid via the transformer.

For the full scale power converter of PMSG wind turbine, the key of grid connection is the GSC control strategy, which generally needs to meet two basic principle: first, to maintain the stability of DC-Link voltage. The second is to realize the control of output phase current. The relationship between the output power of the full scale converter and the wind speed can be expressed as follows:

$$P_{\mathrm{GSC}} \approx \frac{1}{2}\rho A v^3 C_{\mathrm{p}} k, \tag{1}$$

Where P_{GSC} is the output power of GSC, ρ is the air density in $\mathrm{kg/m^3}$, A is the sweep area of the blades in $\mathrm{m^2}$, v is the wind speed in $\mathrm{m/s}$, C_{p} is the power coefficient of the blade, k is the power conversion coefficient.

When the control strategy of the GSC and the load parameters are certain, the effective value of the output line voltage $U_{AB/BC/CA}$ and the phase current $I_{A/B/C}$ can be calculated by the DC-Link voltage:

$$U_{AB/BC/CA} = \sqrt{\frac{1}{2\pi}\int_0^{2\pi} u_{AB/BC/CA}^2 d\omega t} = 0.816 U_d \tag{2}$$

,

$$I_{A/B/C} = \frac{P_{GSC}}{\sqrt{3} U_{AB/BC/CA} \cos\varphi}, \tag{3}$$

Where $u_{AB/BC/CA}$ is the output line voltage of GSC; U_d is the DC-Link voltage; $\cos\varphi$ is power factor of a phase load. In the actual operation of wind turbine, the voltage U_{d}, $U_{AB/BC/CA}$ are constant by the function of control strategy of converter. As can be observed from (1) to (3), phase current $I_{A/B/C}$ of GSC is nearly a cubic function of the wind speed v when the other parameters are invariant. It can be stated that the phase current is random and unstable. Thus, it is difficult to diagnose the open-circuit fault, which is also one of the most significant differences between the wind turbine converter and other converters.

2.2. Faults Analysis with GSC

Most of the existing open-circuit fault diagnosis strategies of power converter are only concerning the single open-circuit failure state. However, the larger current or peak of voltage would break down another IGBT module, result in a double open-circuit faults of the IGBT modules, if the

Preprints (www.preprints.org) | NOT PEER-REVIEWED | Posted: 26 February 2020 doi:10.20944/preprints202002.0392.v1

Peer-reviewed version available at Appl. Sci. 2020, 10, 2146; doi:10.3390/app10062146

system failed to respond in time to cut off the electric energy transmission after the occurrence of single open-circuit fault. Therefore, this paper is considering the single and double IGBT modules open-circuit faults of GSC. Then, there are 22 open-circuit failure states including 1 normal operating state for the 6 IGBT models of GSC. The code of IGBT modules open-circuit fault of GSC is shown in Table 1.

Table 1. Code of open-circuit fault of IGBT modules.

Fault Type Description	T6	T5	T4	T3	T2	T1	Coding Number
Normal	0	0	0	0	0	0	1
Single open-circuit	0	0	0	0	0	1	2
	0	0	0	0	1	0	3
	0	0	0	1	0	0	4
	0	0	1	0	0	0	5
	0	1	0	0	0	0	6
	1	0	0	0	0	0	7
Double open-circuit in the same phase	0	0	1	0	0	1	8
	0	1	0	0	1	0	9
	1	0	0	1	0	0	10
Double upper open-circuit in the different phases	0	0	0	1	0	1	11
	0	1	0	0	0	1	12
	0	1	0	1	0	0	13
Double lower open-circuit in the different phases	0	0	1	0	1	0	14
	1	0	0	0	1	0	15
	1	0	1	0	0	0	16
Upper and lower open-circuit in the different phases, respectively	0	0	0	0	1	1	17
	0	0	0	1	1	0	18
	0	0	1	1	0	0	19
	0	1	1	0	0	0	20
	1	1	0	0	0	0	21
	1	0	0	0	0	1	22

Where T1, T2, T3, T4, T5 and T6 represent the corresponding IGBT modules in Figure 1. The value of Ti (i=1, 2, …, 6) are the states of IGBT modules. When the value of Ti is equal to 0, it means that Ti is operating normally at this time. When the value of Ti is equal to 1, it means that Ti is open-circuit fault at this time. The 1 to 22 are the coding number correspond to the each failure state of the IGBT modules. For instance, code 2 is correspond to 000001, which means that the T1 IGBT module is single open-circuit, other IGBT modules are normal at this time. Code 21 is correspond to 110000, which means that the T5 and T6 IGBT modules are double open-circuit, other IGBT modules are normal. According to the Table 1, technicians can clearly locate which IGBT modules in the GSC have open-circuit faults.

3. Fault Diagnosis Method

3.1. VMD Modeling

The target of VMD is to decompose a real valued input signal f into a discrete number of sub-signal u_k, that have specific sparsity properties while reproducing the input. Assuming each mode u_k to be mostly compact around a center pulsation ω_k, which is to be determined along with the decomposition [22,23]. A scheme to assess the bandwidth of a mode is as follows: 1, for each mode u_k, compute the associated analytic signal by means of the Hilbert transform in order to obtain a unilateral frequency spectrum. 2, for each mode, shift the mode's frequency spectrum to "baseband", by mixing with an exponential tuned to the respective estimated center frequency. 3, the bandwidth

is now estimated through the H^1 Gaussian smoothness of the demodulated signal, the squared 2-norm of the gradient. The resulting constrained variational problem is as follows:

$$\min_{\{u_k\},\{\omega_k\}} \left\{ \sum_k \left\| \partial_t \left[\left(\delta(t) + \frac{j}{\pi t} \right) u_k(t) \right] e^{-j\omega_k t} \right\|_2^2 \right\} \quad \text{s. t.} \ \sum_k u_k = f, \tag{4}$$

Where $\{u_k\} = \{u_1, \cdots, u_K\}$ is all modes. $\{\omega_k\} = \{\omega_1, \cdots, \omega_K\}$ is center frequencies of all modes. K is the number of levels of decomposition.

In order to render the problem unconstrained, a quadratic penalty term and Lagrangian multipliers λ are both used. The augmented Lagrangian L is as follows:

$$L(\{u_k\},\{\omega_k\},\lambda) = \alpha \sum_k \left\| \partial_t \left[\left(\delta(t) + \frac{j}{\pi t} \right) u_k(t) \right] e^{-j\omega_k t} \right\|_2^2 + \left\| f(t) - \sum_k u_k(t) \right\|_2^2 + \left\langle \lambda(t), f(t) - \sum_k u_k(t) \right\rangle \tag{5}$$

,

Minimization u_k and ω_k, respectively:

$$\hat{u}_k^{n+1}(\omega) = \frac{\hat{f}(\omega) - \sum_{i \neq k} \hat{u}_i(\omega) + 0.5\hat{\lambda}(\omega)}{1 + 2\alpha(\omega - \omega_k)^2} \tag{6}$$

,

$$\omega_k^{n+1} = \frac{\int_0^\infty \omega \left| \hat{u}_k(\omega) \right|^2 d\omega}{\int_0^\infty \left| \hat{u}_k(\omega) \right|^2 d\omega}, \tag{7}$$

The decomposition procedure of VMD method is as follows:

Step 1. Initialize $\{\hat{u}_k^1\}, \{\omega_k^1\}, \hat{\lambda}^1, n \leftarrow 0$.

Step 2. Update u_k, ω_k and λ, $n \leftarrow n+1$, $k = 1:K$.

$$\hat{u}_k^{n+1}(\omega) \leftarrow \frac{\hat{f}(\omega) - \sum_{i<k} \hat{u}_i^{n+1}(\omega) - \sum_{i>k} \hat{u}_i^n(\omega) + 0.5\hat{\lambda}^n(\omega)}{1 + 2\alpha(\omega - \omega_k^n)^2}, (\omega \geq 0), \tag{8}$$

$$\omega_k^{n+1} \leftarrow \frac{\int_0^\infty \omega \left| \hat{u}_k^{n+1}(\omega) \right|^2 d\omega}{\int_0^\infty \left| \hat{u}_k^{n+1}(\omega) \right|^2 d\omega}, \tag{9}$$

$$\hat{\lambda}^{n+1}(\omega) \leftarrow \hat{\lambda}^n(\omega) + \tau \left(\hat{f}(\omega) - \sum_k \hat{u}_k^{n+1}(\omega) \right), (\omega \geq 0), \tag{10}$$

Step 3. Repeat the iterative procedure of Step 2 until,

$$\frac{\sum_k \left\| \hat{u}_k^{n+1} - \hat{u}_k^n \right\|_2^2}{\left\| \hat{u}_k^n \right\|_2^2} < \varepsilon, \tag{11}$$

Where ε is a given parameter.

3.2. Trend Feature Analysis of Decomposed Data

A novel method of trend feature analysis is proposed for extracting trend feature vectors in this part. The three-phase current $I_{A/B/C}$ varying with wind speed v of GSC under 22 failure states are decomposed by variational mode in K levels, and each phase current gets K levels of modes:

$$A_{xu}=\{A_{xu1},\ \cdots,\ A_{xuK}\}, \tag{12}$$

$$B_{xu}=\{B_{xu1},\ \cdots,\ B_{xuK}\}, \tag{13}$$

$$C_{xu}=\{C_{xu1},\ \cdots,\ C_{xuK}\}, \tag{14}$$

Where A, B and C denote the each phase of GSC in Figure 1; $x=1,2,\cdots,22$ denotes fault code; A_{xu}, B_{xu} and C_{xu} are the modes sets of three-phase current after decomposing; A_{xuk}, B_{xuk} and C_{xuk} ($k=1,2,...,K$) are the k -th mode coefficient series of three-phase current modes sets, respectively.

Extracting E_{Axk}, E_{Bxk} and E_{Cxk} the feature energy of each mode of three-phase current can be expressed as:

$$E_{Axkj}=\sum_{j=1}^{n}\left|A_{xuk}(j)\right|^2,\ x=1,2,\cdots,22,\ k=1,2,...,K, \tag{15}$$

$$E_{Bxkj}=\sum_{j=1}^{n}\left|B_{xuk}(j)\right|^2,\ x=1,2,\cdots,22,\ k=1,2,...,K, \tag{16}$$

$$E_{Cxkj}=\sum_{j=1}^{n}\left|C_{xuk}(j)\right|^2,\ x=1,2,\cdots,22,\ k=1,2,...,K, \tag{17}$$

Where E_{Axk}, E_{Bxk} and E_{Cxk} are the feature energy of each mode of three-phase current, respectively. n is the total number of coefficients at each mode coefficient series.

The each open-circuit fault of IGBT modules would have a great impact on the feature energy in each mode of three-phase current. Therefore, the feature energy vectors E_A, E_B and E_C could be constructed by the feature energy of each mode.

$$E_{Ax}=\left[E_{Ax1}\quad E_{Ax2}\quad ...\quad E_{AxK}\right],\ x=1,2,\cdots,22, \tag{18}$$

$$E_{Bx}=\left[E_{Bx1}\quad E_{Bx2}\quad ...\quad E_{BxK}\right],\ x=1,2,\cdots,22, \tag{19}$$

$$E_{Cx}=\left[E_{Cx1}\quad E_{Cx2}\quad ...\quad E_{CxK}\right],\ x=1,2,\cdots,22, \tag{20}$$

The three-phase current vary according to the wind speed. The same varieties occur to the feature energy of each mode. Thus, when the open-circuit happens in the GSC, the varied feature energy vectors would bring difficulties to the following data analysis. It is necessary to normalize the feature energy vectors. Let:

$$F_{Axk}=\frac{E_{Axk}}{\sum_{l=1}^{K}E_{Axl}+\sigma},\ x=1,2,\cdots,22,\ k=1,2,...,K, \tag{21}$$

$$F_{Bxk}=\frac{E_{Bxk}}{\sum_{l=1}^{K}E_{Bxl}+\sigma},\ x=1,2,\cdots,22,\ k=1,2,...,K, \tag{22}$$

$$F_{Cxk}=\frac{E_{Cxk}}{\sum_{l=1}^{K}E_{Cxl}+\sigma},\ x=1,2,\cdots,22,\ k=1,2,...,K, \tag{23}$$

Preprints (www.preprints.org) | NOT PEER-REVIEWED | Posted: 26 February 2020 doi:10.20944/preprints202002.0392.v1

Peer-reviewed version available at Appl. Sci. 2020, 10, 2146; doi:10.3390/app10062146

Where σ is a tiny real number to avoid the erroneous judgment when the phase current is zero, and minimize impact on final classification results. The normalized feature energy vectors can be expressed as:

$$F_{Ax} = \begin{bmatrix} F_{Ax1} & F_{Ax2} & \cdots & F_{AxK} \end{bmatrix}, x = 1,2,\cdots,22, \tag{24}$$

$$F_{Bx} = \begin{bmatrix} F_{Bx1} & F_{Bx2} & \cdots & F_{BxK} \end{bmatrix}, x = 1,2,\cdots,22, \tag{25}$$

$$F_{Cx} = \begin{bmatrix} F_{Cx1} & F_{Cx2} & \cdots & F_{CxK} \end{bmatrix}, x = 1,2,\cdots,22, \tag{26}$$

Then, the factors of normalized feature energy vectors can be the function about the part factors of trend feature vectors. Let:

$$I_{x\_k} = (F_{Axk})^{\frac{1}{p}}, x = 1,2,\cdots,22, k = 1,2,\ldots,K, \tag{27}$$

$$I_{x\_k+K} = (F_{Bxk})^{\frac{1}{p}}, x = 1,2,\cdots,22, k = 1,2,\ldots,K, \tag{28}$$

$$I_{x\_k+2K} = (F_{Cxk})^{\frac{1}{p}}, x = 1,2,\cdots,22, k = 1,2,\ldots,K, \tag{29}$$

Where p is a positive real number. The value of p could be confirm in an optimal range through several experiments. $\{I_{x\_1} \quad I_{x\_2} \quad \ldots \quad I_{x\_3K}\}$ is the part factors set of trend feature vectors, which could be used to judge which the phases are open-circuit. To locate the location of open-circuit IGBT module is upper or lower, 3 additional factors of trend feature vectors are needed to add in.

The first level modes of three-phase current are most similar to the original current signals. The coefficient sum of the first level modes of three-phase current can be expressed as:

$$S_{Ax1j} = \sum_{j=1}^{n} A_{xu1}(j), x = 1,2,\cdots,22, \tag{30}$$

$$S_{Bx1j} = \sum_{j=1}^{n} B_{xu1}(j), x = 1,2,\cdots,22, \tag{31}$$

$$S_{Cx1j} = \sum_{j=1}^{n} C_{xu1}(j), x = 1,2,\cdots,22, \tag{32}$$

Where S_{Ax1}, S_{Bx1} and S_{Cx1} are the coefficient sum of the first level modes of three-phase current. n is the total number of coefficients at each mode coefficient series.

Define I_{x_3K+1}, I_{x_3K+2} and I_{x_3K+3} are the 3 additional factors of trend feature vectors. Let:

$$I_{x\_3K+1} = \begin{cases} 1 & , \quad S_{Ax1} > 0 \\ 0 & , \quad S_{Ax1} = 0, x = 1,2,\cdots,22, \\ -1 & , \quad S_{Ax1} < 0 \end{cases} \tag{33}$$

$$I_{x\_3K+2} = \begin{cases} 1 & , \quad S_{Bx1} > 0 \\ 0 & , \quad S_{Bx1} = 0, x = 1,2,\cdots,22, \\ -1 & , \quad S_{Bx1} < 0 \end{cases} \tag{34}$$

Preprints (www.preprints.org) | NOT PEER-REVIEWED | Posted: 26 February 2020 doi:10.20944/preprints202002.0392.v1

Peer-reviewed version available at Appl. Sci. 2020, 10, 2146; doi:10.3390/app10062146

$$I_{x\_3K+3}=\begin{cases}1 & , \quad S_{Cx1}>0\\ 0 & , \quad S_{Cx1}=0\\ -1 & , \quad S_{Cx1}<0\end{cases}, x=1,2,\cdots,22, \tag{35}$$

Then, the trend feature vectors of x-th failure state is:

$$I_x=\begin{bmatrix}I_{x\_1} & I_{x\_2} & \ldots & I_{x\_3K+3}\end{bmatrix}, x=1,2,\cdots,22, \tag{36}$$

Where $3K+3$ is the number of factors in each trend feature vectors.

3.3. DBN Modeling

In 2006, a DBN model with a efficient learning algorithm proposed by Geoffrey Hinton. This algorithm becomes the main framework of the deep learning algorithm later. It can extract the required features from the training set automatically [24,25]. The typical model is the restricted Boltzmann machine (RBM). The features extracted automatically solve the careless factors in the manual extraction, and initialize the weights of neural network. Then Softmax function can be used to classify, and contributes good experimental results. DBN can be composed of multi-layer RBM. A typical DBN model with double-layer RBM is shown in the Figure 2.

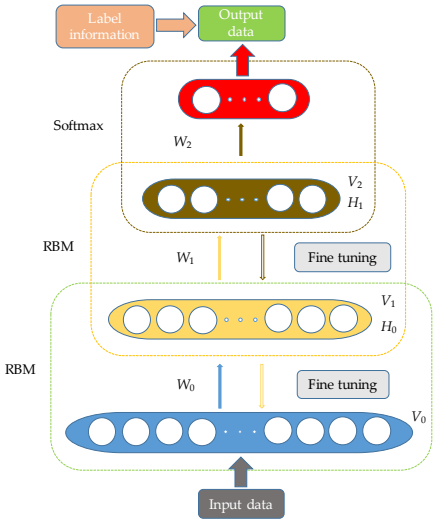

FIGURE 2. DBN model with double-layer RBM.

The process of DBN training model can be mainly divided into two steps.

Step 1: Unsupervised pretraining. Each layer of RBM network is trained independently and unsupervised to ensure that as much feature information as possible is preserved when the feature vectors are mapped to different feature spaces. The greedy method is adopted between the layers training, and the process is as follows:

1. The input layer V_0 of the first RBM is also the input layer of the entire network. It typically involves training the first layer RBM by applying contrastive divergence. W_0 is the weight in the first RBM.
2. The hidden layer H_0 of the previous layer RBM can be seen as the visible layer V_1 of the back layer RBM, followed by iterative training remaining RBM. W_1 is the weight in the back layer RBM.

3.4. Mission Profile of the Method

Figure 3 shows the whole process of open-circuit fault diagnosis with proposed novel method, including VMD, trend feature analysis and DBN algorithm. Above all, the three-phase current varying with wind speed of IGBT modules open-circuit of GSC are extracted under 22 failure states. Afterward, the three-phase current are conducted by VMD at K levels to obtain the corresponding

modes. Trend feature analysis is proposed to address the corresponding modes data to produce the trend feature vectors under 22 failure states. Finally, input the trend feature vectors to DBN, which is used to train and test and construct the model, and obtain the classification results.

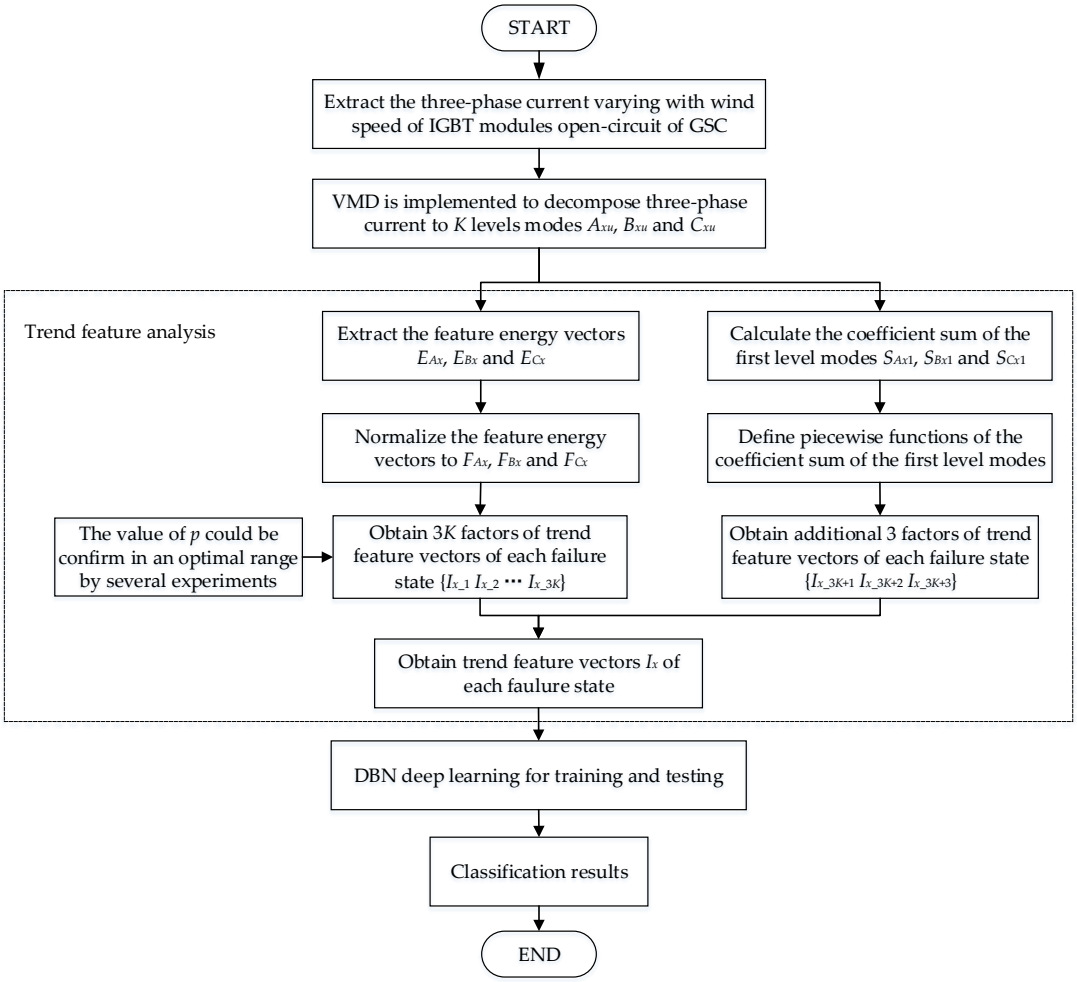

Figure 3. The mission profile of open-circuit fault diagnosis with proposed novel method

4. Simulation Results

The simulation results produced from the proposed method which is addressed to diagnose the open-circuit faults of GSC are evaluated in this section.

Simulink is used to simulate 22 failure states of GSC of PMSG wind turbine, as shown in Figure 3. The three-phase current I_A, I_B and I_C varying with wind speed are extracted, where the subscripts A, B and C are the each phase. Extracting 1000 samples under each failure state. The length of time of each sample is between T and $1.15T$, where T is the period of the phase current. 800 samples out of 1000 samples under each failure state are randomly selected to compose training set, and the remaining 200 samples are used to compose test set. So, the sum of entire samples is 22000, including 17600 in training set and 4400 in test set.

Preprints (www.preprints.org) | NOT PEER-REVIEWED | Posted: 26 February 2020 doi:10.20944/preprints202002.0392.v1

Peer-reviewed version available at Appl. Sci. 2020, 10, 2146; doi:10.3390/app10062146

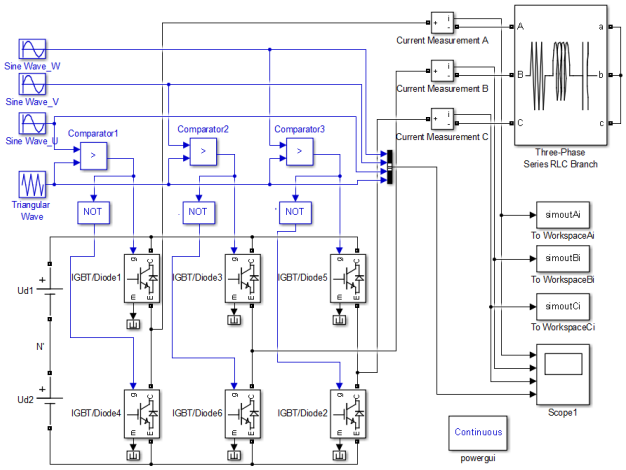

Figure 3. Simulation block diagram of GSC.

Table 2 is the parameters of main simulation components.

Table 2. Parameters of simulation components.

Item	Parameter Value
U_{d}	$1050V$
$U_{AB/BC/CA}$	$690V$
Voltage of sine wave	$0.7V$
Frequency of sine wave	50Hz
Frequency of triangular wave	1000Hz
Phase difference of each phase	120°

4.1. VMD of Three-phase Current

Considering [26], the whole three-phase current samples under 22 failure states are addressed by VMD at 7 levels. Figure 4 and Figure 5 show the waveforms of three-phase current and the mode coefficient serials under No. 1 (normal operating) and No. 2 failure states, respectively. Where the red, green and blue curves denote the A, B and C phase current in Figure 4 and Figure 5, respectively.

1. No. 1 failure state (normal operating).

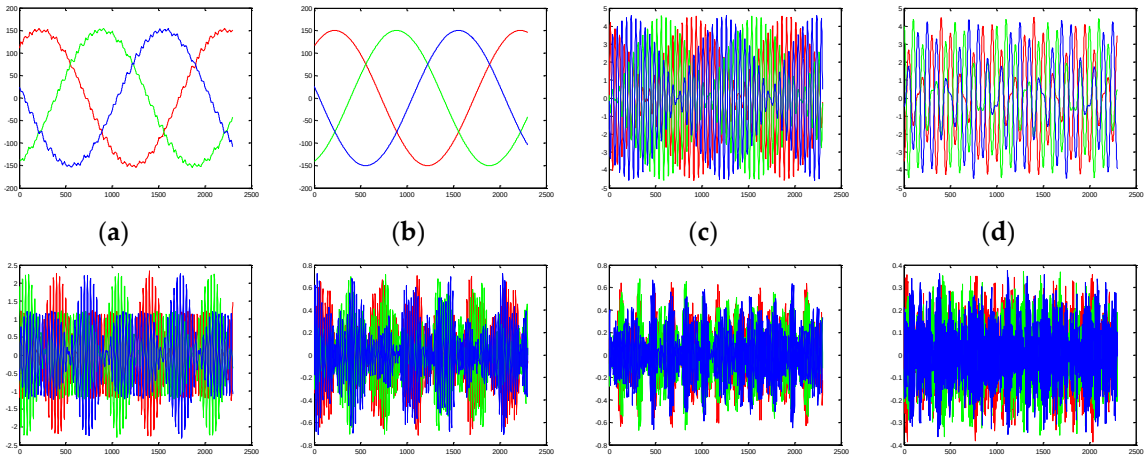

Figure 4. Waveforms of three-phase current and the mode coefficients serials under No. 1 failure state. (a) Waveform of three-phase current. (b) - (h) Waveforms of mode coefficients serials from 1st level to 7th level.

Preprints (www.preprints.org) | NOT PEER-REVIEWED | Posted: 26 February 2020 doi:10.20944/preprints202002.0392.v1

Peer-reviewed version available at Appl. Sci. 2020, 10, 2146; doi:10.3390/app10062146

It can be seen from Figure 4 (a) that there is no phase sequence alteration, meanwhile, three-phase current is operating on a stable state. Figure 4 (b)-(h) show that the waveforms of modes are relatively balanced. The feature energy of each mode decreases from the first level to seventh level. The majority feature energy is in the first level.

2. No. 2 failure state. The T1 IGBT module is open-circuit in phase-A.

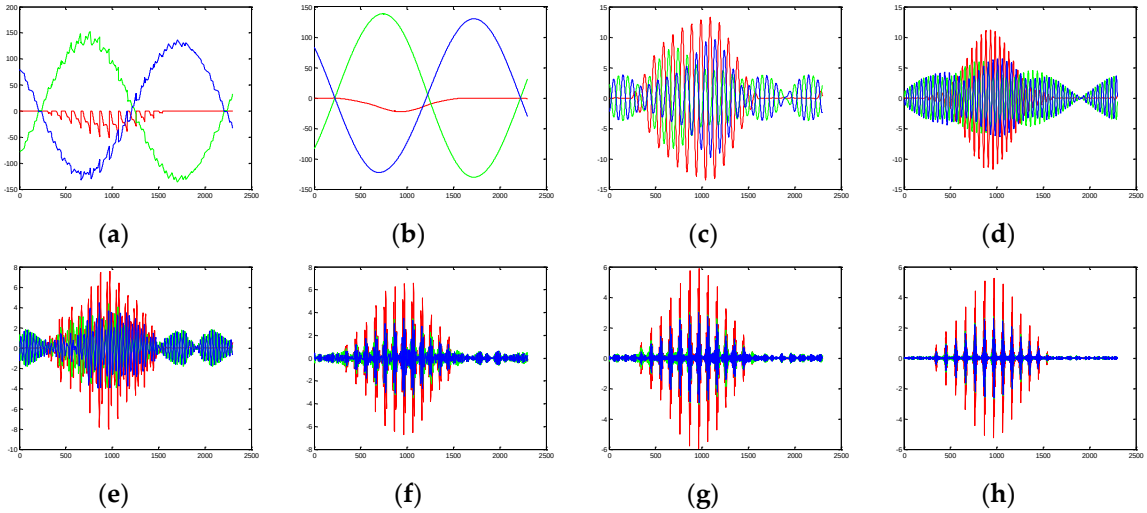

Figure 5. Waveforms of three-phase current and the mode coefficients serials under No. 2 failure state. (a) Waveform of three-phase current. (b) - (h) Waveforms of mode coefficients serials from 1st level to 7th level.

It can be seen from Figure 5 (a) that the value of phase-A current is non positive when T1 IGBT module is open-circuit. This is determined by the electrical structure and working principle of GSC. The currents of phase-B and phase-A are stable but changed in phase sequences, almost reverses for each other. Figure 5 (b)-(h) show the feature energy of each level altered in phase-A modes. The proportion of feature energy of first level in phase-A is reduced. But the proportion of feature energy of other levels in phase-A are increased. The proportion of feature energy of levels of phase-B and phase-C are not sensitive to change.

4.2. Using Trend Feature Analysis to Extract Trend Feature Vectors

The trend feature analysis is conducted to analyze the modes coefficients serials by using (12)-(36) in Section 3. The trend feature vectors under 22 open-circuit failure states are shown in Table 3.

Table 3. The trend feature vectors under 22 open-circuit failure states of GSC.

Coding Number	1	2	3	4	...	18	19	20	21	22
I_{x_1}	0.9435	0.4281	0.9139	0.8947		0.6465	0.3872	0.4256	0.6481	0.3891
I_{x_2}	0.0217	0.2180	0.0312	0.0412		0.1343	0.2487	0.2414	0.1332	0.2582
I_{x_3}	0.0204	0.1466	0.0268	0.0304		0.0880	0.1559	0.1426	0.0845	0.1443
I_{x_4}	0.0082	0.0842	0.0121	0.0153		0.0568	0.0844	0.0735	0.0593	0.0845
I_{x_5}	0.0026	0.0557	0.0074	0.0084		0.0339	0.0567	0.0533	0.0339	0.0561
I_{x_6}	0.0022	0.0396	0.0050	0.0059		0.0238	0.0393	0.0369	0.0239	0.0396
I_{x_7}	0.0013	0.0278	0.0034	0.0041		0.0167	0.0278	0.0266	0.0170	0.0281
I_{x_8}	0.9489	0.9210	0.9099	0.4280		0.4008	0.4194	0.6516	0.3887	0.4181
I_{x_9}	0.0197	0.0289	0.0339	0.2190		0.2537	0.2323	0.1291	0.2620	0.2411
I_{x_10}	0.0183	0.0236	0.0270	0.1469		0.1410	0.1517	0.0893	0.1420	0.1433
I_{x_11}	0.0074	0.0119	0.0135	0.0837		0.0833	0.0761	0.0559	0.0843	0.0778
I_{x_12}	0.0024	0.0068	0.0072	0.0557	…	0.0551	0.0551	0.0336	0.0558	0.0544
I_{x_13}	0.0020	0.0047	0.0050	0.0389		0.0386	0.0381	0.0236	0.0392	0.0383
I_{x_14}	0.0012	0.0031	0.0035	0.0279		0.0276	0.0273	0.0168	0.0279	0.0270

Preprints (www.preprints.org) | NOT PEER-REVIEWED | Posted: 26 February 2020 doi:10.20944/preprints202002.0392.v1

Peer-reviewed version available at Appl. Sci. 2020, 10, 2146; doi:10.3390/app10062146

I_{x_15}	0.9478	0.9169	0.4226	0.9094	0.4116	0.6359	0.3831	0.4155	0.6470
I_{x_16}	0.0198	0.0316	0.2236	0.0322	0.2471	0.1384	0.2647	0.2479	0.1327
I_{x_17}	0.0185	0.0247	0.1443	0.0265	0.1424	0.0864	0.1432	0.1394	0.0868
I_{x_18}	0.0083	0.0124	0.0858	0.0137	0.0788	0.0616	0.0850	0.0781	0.0581
I_{x_19}	0.0023	0.0066	0.0562	0.0084	0.0549	0.0354	0.0563	0.0542	0.0342
I_{x_20}	0.0021	0.0045	0.0396	0.0057	0.0382	0.0247	0.0395	0.0379	0.0241
I_{x_21}	0.0012	0.0032	0.0280	0.0040	0.0271	0.0176	0.0282	0.0270	0.0170
I_{x_22}	1	-1	1	-1	1	1	1	1	-1
I_{x_23}	-1	-1	-1	-1	-1	-1	-1	1	1
I_{x_24}	1	1	1	1	1	1	-1	-1	-1

Where the subscripts x denotes the coding number. For instance, the trend feature vectors of No. 1 failure is I_1=[0.9435 0.0217 … 1] when x=1. The trend feature vectors of No. 21 failure is I_{21}=[0.6481 0.1332 … 1] when x=21.

4.3. DBN Training and Test Recults Analysis

In this paper, the input of DBN under each open-circuit failure state is a 24 dimensions trend feature vectors $I_x = \left[I_{x\_1} \quad I_{x\_2} \quad \cdots \quad I_{x\_24} \right]$, $x = 1, 2, \cdots, 22$,where x denotes the failure coding number. The DBN consists of double-layer RBM and Softmax classifier. In order to reduce the dimensions and retain the feature information of the trend feature vectors, the number of neurons in the first layer of RBM is set to 14, and the number of neurons in the second layer of RBM is set to 5. Then, the input of Softmax classifier is 5 dimensions. The output of Softmax classifier is a 22 dimensions probability vectors $S = \left[S_1 \quad S_2 \quad \cdots \quad S_{22} \right]$, where S_j ($j = 1, 2, \cdots, 22$) denots the probability of the j-th fault. Table 4 shows the probability output results of Softmax classifier and corresponding failure coding number.

Table 4. The probability output results of Softmax and corresponding failure coding number.

Coding Number	1	2	3	…	19	20	21	22
S_1	0.999990	0.000000	0.000000		0.000000	0.000000	0.000000	0.000000
S_2	0.000000	0.999999	0.000000		0.000000	0.000000	0.000000	0.000001
S_3	0.000001	0.000000	0.999998		0.000000	0.000000	0.000000	0.000000
S_4	0.000007	0.000000	0.000000		0.000000	0.000000	0.000000	0.000000
S_5	0.000001	0.000000	0.000000		0.000000	0.000000	0.000000	0.000000
S_6	0.000000	0.000000	0.000000		0.000000	0.000000	0.000000	0.000000
S_7	0.000000	0.000000	0.000000		0.000000	0.000000	0.000000	0.000000
S_8	0.000000	0.000000	0.000000		0.000000	0.000000	0.000000	0.000000
S_9	0.000001	0.000000	0.000000		0.000000	0.000000	0.000000	0.000000
S_{10}	0.000000	0.000000	0.000000		0.000000	0.000000	0.000000	0.000000
S_{11}	0.000000	0.000000	0.000000		0.000000	0.000000	0.000000	0.000000
S_{12}	0.000000	0.000000	0.000000	…	0.000000	0.000000	0.000000	0.000001
S_{13}	0.000000	0.000000	0.000000		0.000000	0.000001	0.000000	0.000000
S_{14}	0.000000	0.000000	0.000000		0.000003	0.000000	0.000000	0.000000
S_{15}	0.000000	0.000000	0.000000		0.000000	0.000000	0.000000	0.000000
S_{16}	0.000000	0.000000	0.000000		0.000000	0.000000	0.000001	0.000000
S_{17}	0.000000	0.000000	0.000000		0.000000	0.000000	0.000000	0.000000
S_{18}	0.000000	0.000000	0.000001		0.000000	0.000000	0.000000	0.000000
S_{19}	0.000000	0.000000	0.000000		0.999996	0.000000	0.000000	0.000000
S_{20}	0.000000	0.000000	0.000000		0.000000	0.999997	0.000000	0.000000
S_{21}	0.000000	0.000000	0.000000		0.000000	0.000000	0.999998	0.000000
S_{22}	0.000000	0.000000	0.000000		0.000000	0.000000	0.000000	0.999997

Table 4 shows that, for instance, put the No. 1 trend feature vectors into DBN model, the classification result is S=[0.999990 0.000000 … 0.000000], which means the probability of No. 1 trend

Preprints (www.preprints.org) | NOT PEER-REVIEWED | Posted: 26 February 2020 doi:10.20944/preprints202002.0392.v1

Peer-reviewed version available at Appl. Sci. 2020, 10, 2146; doi:10.3390/app10062146

feature vectors belonging to No. 1 failure state is 99.999%. put the No. 22 trend feature vectors into DBN model, the classification result is S=[0.000000 0.000001 … 0.999997], which means the probability of No. 22 trend feature vectors belonging to No. 22 failure state is 99.9997%. Table 4 verifies the simulation classification results generated from the proposed method are accurate to the failure coding number, if the accurate standard is upper than 50%.

To compare the performance of proposed method, the other 7 methods are involved to address the same samples. The total 8 methods are: 1, proposed method, VMD, trend feature and DBN (VMD-TFA-DBN); 2, VMD, trend feature analysis and back propagation neural network (BPNN) (VMD-TFA-BP); 3, trend feature analysis and DBN (TFA-DBN); 4, trend feature analysis and BPNN (TFA-BP); 5, VMD and DBN (VMD-DBN); 6, VMD and BPNN (VMD-BP); 7, only DBN (DBN); 8, only BPNN (BP). To increase the credibility, every method trains the same training set and tests the same test set at 100 times. Table 5 shows the comparison results between 8 methods.

Table 5. The simulation comparison results of open-circuit fault diagnosis under 8 methods.

Open-circuit fault diagnosis methods	Accuracy	Error Times
VMD-TFA-DBN	100%	0
VMD-TFA-BP	93.26%	29656
TFA-DBN	95.45%	20020
TFA-BP	63.57%	160292
VMD-DBN	20.69%	348964
VMD-BP	16.78%	366168
DBN	18.18%	360008
BP	3.75%	423500

The following conclusions can be analyzed and drawn from Table 5:

1. The method of VMD-TFA-DBN, proposed in this paper, has generated the best classifying capability under the 22 circumstances that the accuracy is 100%, the error times is 0.
2. The method of only BP has produced the worst classifying performance, the accuracy is 3.75%, the error times is 423500.
3. When the accuracy of VMD-TFA-DBN is higher than VMD-TFA-BP, TFA-DBN is higher than TFA-BP, VMD-DBN is higher than VMD-BP, and DBN is higher than BP. All of these illustrate the classification accuracy of DBN in higher than BP in the models.
4. The accuracy of each method used proposed TFA is higher than corresponding who does not use TFA, which verifies the great function of TFA for increasing classification accuracy.
5. The accuracy of each method used VMD is higher than corresponding who does not use VMD, which verifies the function of VMD in proposed method.

5. Experimental Results

In this section, experimental results are generated to verify the simulation results and analysis. As the same as simulation, the three-phase current I_A, I_B and I_C are extracted, where the subscripts A, B and C are the each phase. Extracting 1000 samples under each failure state. The length of time of each sample is between T and $1.15T$, where T is the period of the phase current. 800 samples out of 1000 samples under each failure state are randomly selected to compose training set, and the remaining 200 samples are used to compose test set. So, the sum of entire samples is 22000, including 17600 in training set and 4400 in test set.

Table 6 is the parameters of main components of GSC.

Table 6. Parameters of main components of GSC.

Item	Parameter Value
U_{d}	$1050V$
$U_{AB/BC/CA}$	$690V$
Voltage of sine wave	$0.7V$
Frequency of sine wave	50Hz
Frequency of triangular wave	1000Hz

Phase difference of each phase	120°

5.1. VMD of Three-phase Current

The whole three-phase current samples under 22 failure states are addressed by VMD at 7 levels. Figure 6 and Figure 7 show the waveforms of phase-A current and the mode coefficient serials under No. 1 (normal operating) and No. 2 failure states, respectively.

1. No. 1 failure state (normal operating).

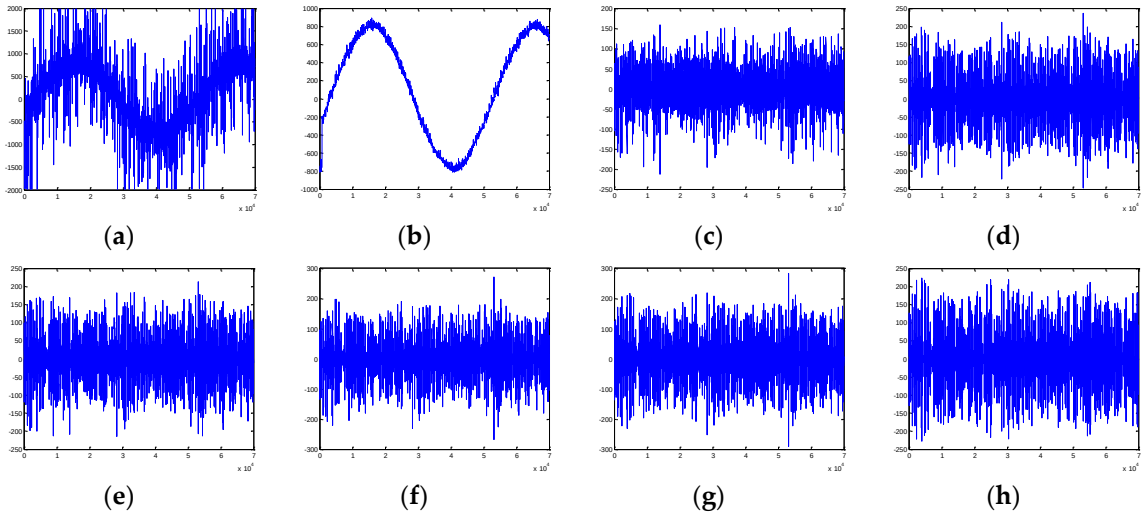

Figure 6. Waveforms of phase-A current and the mode coefficients serials under No. 1 failure state. (a) Waveform of phase-A current. (b) - (h) Waveforms of mode coefficients serials from 1st level to 7th level.

It can be seen from Figure 6 (a) that the waveforms of phase is stable as same as each phase in Figure 4 (a). Figure 6 (b)-(h) show that the feature energy of each mode decreases from the first level to seventh level. The majority feature energy is in the first level.

2. No. 2 failure state. The T1 IGBT module is open-circuit in phase-A.

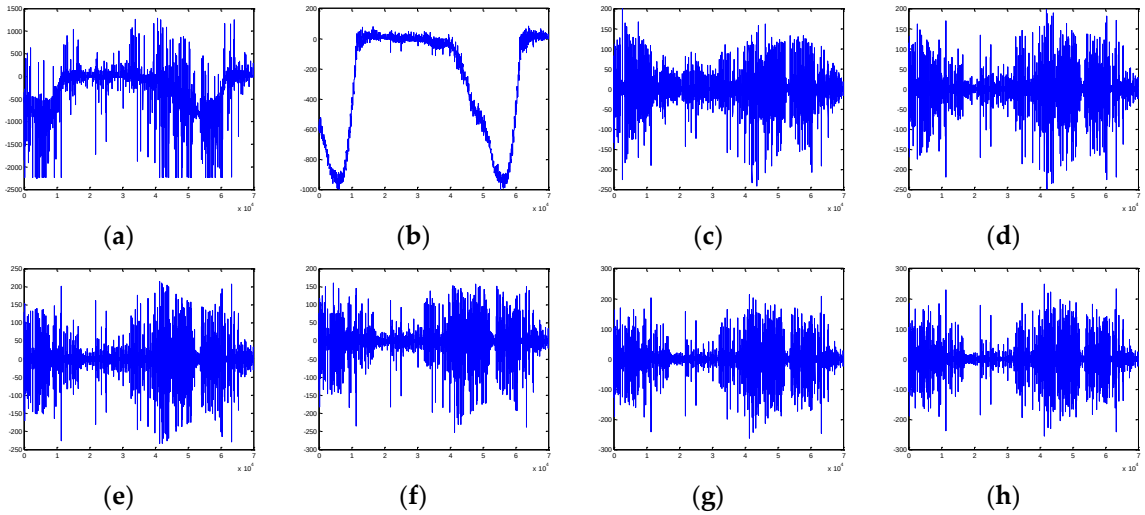

Figure 7. Waveforms of phase-A current and the mode coefficients serials under No. 2 failure state. (a) Waveform of phase-A current. (b) - (h) Waveforms of mode coefficients serials from 1st level to 7th level.

It can be seen from Figure 7 that the waveforms of phase-A is similar (to red curve) in Figure 5. The value of phase-A current is non positive for a large majority. Figure 7 (b)-(h) show the feature

Preprints (www.preprints.org) | NOT PEER-REVIEWED | Posted: 26 February 2020 doi:10.20944/preprints202002.0392.v1

Peer-reviewed version available at Appl. Sci. 2020, 10, 2146; doi:10.3390/app10062146

energy of each level altered. The proportion of feature energy of first level is reduced. But the proportion of feature energy of other levels are increased.

5.2. Using Trend Feature Analysis to Extract Trend Feature Vectors

The trend feature vectors under 22 open-circuit failure states are shown in Table 7.

Table 7. The trend feature vectors under 22 open-circuit failure states of GSC.

Coding Number	1	2	3	4	...	18	19	20	21	22
I_{x_1}	0.9434	0.4281	0.9144	0.8946		0.6474	0.3872	0.4253	0.6489	0.3891
I_{x_2}	0.0218	0.2180	0.0311	0.0413		0.1342	0.2473	0.2408	0.1329	0.2582
I_{x_3}	0.0205	0.1466	0.0267	0.0303		0.0874	0.1558	0.1435	0.0844	0.1443
I_{x_4}	0.0082	0.0842	0.0121	0.0153		0.0568	0.0849	0.0739	0.0592	0.0845
I_{x_5}	0.0026	0.0557	0.0073	0.0085		0.0338	0.0570	0.0532	0.0338	0.0561
I_{x_6}	0.0022	0.0396	0.0050	0.0059		0.0238	0.0397	0.0369	0.0239	0.0396
I_{x_7}	0.0013	0.0278	0.0034	0.0041		0.0167	0.0281	0.0265	0.0169	0.0281
I_{x_8}	0.9492	0.9210	0.9103	0.4272		0.4010	0.4181	0.6511	0.3890	0.4181
I_{x_9}	0.0195	0.0289	0.0339	0.2199		0.2540	0.2329	0.1291	0.2620	0.2411
I_{x_10}	0.0183	0.0235	0.0269	0.1461		0.1403	0.1513	0.0897	0.1419	0.1433
I_{x_11}	0.0074	0.0119	0.0134	0.0839		0.0833	0.0765	0.0561	0.0843	0.0778
I_{x_12}	0.0024	0.0068	0.0071	0.0559	…	0.0551	0.0554	0.0336	0.0558	0.0544
I_{x_13}	0.0020	0.0047	0.0049	0.0391		0.0387	0.0383	0.0237	0.0392	0.0383
I_{x_14}	0.0012	0.0032	0.0035	0.0280		0.0276	0.0275	0.0168	0.0279	0.0270
I_{x_15}	0.9477	0.9170	0.4230	0.9092		0.4121	0.6350	0.3825	0.4164	0.6471
I_{x_16}	0.0199	0.0316	0.2240	0.0323		0.2471	0.1385	0.2646	0.2475	0.1328
I_{x_17}	0.0186	0.0247	0.1446	0.0265		0.1422	0.0865	0.1437	0.1392	0.0868
I_{x_18}	0.0083	0.0124	0.0854	0.0137		0.0786	0.0617	0.0852	0.0780	0.0581
I_{x_19}	0.0023	0.0066	0.0559	0.0084		0.0548	0.0356	0.0563	0.0541	0.0342
I_{x_20}	0.0021	0.0046	0.0393	0.0057		0.0381	0.0249	0.0395	0.0378	0.0241
I_{x_21}	0.0012	0.0032	0.0278	0.0040		0.0271	0.0178	0.0282	0.0270	0.0170
I_{x_22}	1	-1	1	-1		1	1	1	1	-1
I_{x_23}	-1	-1	-1	-1		-1	-1	-1	1	1
I_{x_24}	1	1	1	1		1	1	-1	-1	-1

Where the subscripts x denotes the coding number. For instance, the trend feature vectors of No. 1 failure is I_1=[0.9434 0.0218 … 1] when x=1. The trend feature vectors of No. 22 failure is I_{22}=[0.3891 0.2582 … -1] when x=22.

5.3. DBN Training and Test Recults Analysis

Then, obtain the trend feature vectors $I_x = \left[I_{x\_1} \quad I_{x\_2} \quad \cdots \quad I_{x\_24} \right]$, $x = 1, 2, \cdots, 22$,where x denotes the failure coding number. The DBN consists of double-layer RBM and Softmax classifier. The number of neurons in the first layer of RBM is set to 14, and the number of neurons in the second layer of RBM is set to 5. The output of Softmax classifier is a 22 dimensions probability vectors $S = \left[S_1 \quad S_2 \quad \cdots \quad S_{22} \right]$, where S_j ($j = 1, 2, \cdots, 22$) denotes the probability of the j -th fault. Table 8 shows the probability output results of Softmax classifier and corresponding failure coding number.

Table 8. The probability output results of Softmax and corresponding failure coding number.

Coding Number	1	2	3	…	19	20	21	22
S_1	0.998857	0.000058	0.000016		0.000000	0.000000	0.000000	0.000000
S_2	0.000000	0.999602	0.000000		0.000000	0.000000	0.000000	0.000080
S_3	0.000379	0.000000	0.999668		0.000000	0.000000	0.000000	0.000000
S_4	0.000106	0.000000	0.000000		0.000059	0.000000	0.000000	0.000000

Preprints (www.preprints.org) | NOT PEER-REVIEWED | Posted: 26 February 2020 doi:10.20944/preprints202002.0392.v1

Peer-reviewed version available at Appl. Sci. 2020, 10, 2146; doi:10.3390/app10062146

S_5	0.000130	0.000010	0.000000		0.000063	0.000060	0.000000	0.000000
S_6	0.000000	0.000000	0.000005		0.000000	0.000089	0.000060	0.000000
S_7	0.000000	0.000000	0.000000		0.000000	0.000000	0.000102	0.000044
S_8	0.000254	0.000260	0.000000		0.000000	0.000000	0.000000	0.000000
S_9	0.000183	0.000000	0.000240		0.000000	0.000000	0.000000	0.000000
S_{10}	0.000091	0.000000	0.000000		0.000000	0.000000	0.000000	0.000000
S_{11}	0.000000	0.000000	0.000000		0.000011	0.000000	0.000000	0.000000
S_{12}	0.000000	0.000000	0.000000	…	0.000000	0.000000	0.000000	0.000484
S_{13}	0.000000	0.000000	0.000000		0.000000	0.000470	0.000012	0.000000
S_{14}	0.000000	0.000000	0.000000		0.000713	0.000014	0.000000	0.000000
S_{15}	0.000000	0.000000	0.000000		0.000000	0.000000	0.000001	0.000000
S_{16}	0.000000	0.000000	0.000000		0.000000	0.000000	0.000285	0.000023
S_{17}	0.000000	0.000064	0.000002		0.000000	0.000002	0.000000	0.000000
S_{18}	0.000000	0.000000	0.000068		0.000001	0.000000	0.000003	0.000000
S_{19}	0.000000	0.000002	0.000000		0.999117	0.000000	0.000000	0.000013
S_{20}	0.000000	0.000000	0.000000		0.000000	0.999364	0.000000	0.000000
S_{21}	0.000000	0.000000	0.000000		0.000000	0.000000	0.999536	0.000003
S_{22}	0.000000	0.000003	0.000000		0.000036	0.000000	0.000000	0.999353

Table 8 shows that, for instance, put the No. 1 trend feature vectors into DBN model, the classification result is S=[0.998857 0.000000 … 0.000000], which means the probability of No. 1 trend feature vectors belonging to No. 1 failure state is 99.999%. put the No. 22 trend feature vectors into DBN model, the classification result is S=[0.000000 0.000080 … 0.999353], which means the probability of No. 22 trend feature vectors belonging to No. 22 failure state is 99.9997%. Table 8 verifies the simulation classification results generated from the proposed method are accurate to the failure coding number, if the accurate standard is upper than 50%.

8 compared methods mentioned in the end of Section 4 are used to compare the performance. They are involved to address the same experimental samples. To increase the credibility, every method trains the same training set and tests the same test set at 100 times. Table 9 shows the experimental comparison results between 8 methods.

Table 9. The experimental comparison results of open-circuit fault diagnosis under 8 methods.

Open-circuit fault diagnosis methods	Accuracy	Error Times
VMD-TFA-DBN	99.99%	3
VMD-TFA-BP	91.92%	35532
TFA-DBN	94.73%	23178
TFA-BP	59.16%	179714
VMD-DBN	18.25%	359684
VMD-BP	12.42%	385361
DBN	15.67%	371071
BP	1.37%	433971

The following conclusions can be analyzed and drawn from Table 9:

1. The method of VMD-TFA-DBN, proposed in this paper, has generated the best classifying capability under the 22 circumstances that the accuracy is 99.99%, the error times is 3.
2. The method of only BP has produced the worst classifying performance, the accuracy is 1.37%, the error times is 433971.
3. When the accuracy of VMD-TFA-DBN is higher than VMD-TFA-BP, TFA-DBN is higher than TFA-BP, VMD-DBN is higher than VMD-BP, and DBN is higher than BP. All of these illustrate the classification accuracy of DBN in higher than BP in the models.
4. The accuracy of each method used proposed TFA is higher than corresponding who does not use TFA, which verifies the great function of TFA for increasing classification accuracy.
5. The accuracy of each method used VMD is higher than corresponding who does not use VMD, which verifies the function of VMD in proposed method.

The conclusions of experimental results are broadly in line with what of simulation results. But the performance of each method of experimental results is worse than corresponding method. The probable causes are summarized as follows:

1. Three-phase current is extracted with error or interference. The samples are varying to indistinct, which lead to the accuracy decreased.
2. The total number of experimental samples in training set may be lack of, which leads to the DBN training model leaky.

6. Conclusions

This paper proposes a novel method to diagnosis the single and double IGBT modules open-circuit faults of GSC of the PMSG wind turbine. Above all, three-phase current varying with wind speed are extracted under 22 failure states. Afterward, the three-phase current are conducted by VMD at 7 levels to obtain the corresponding modes. Trend feature analysis is proposed to address the corresponding modes data to produce the trend feature vectors under 22 failure states. Finally, input the trend feature vectors to DBN, which is used to train and test and construct the model, and obtain the classification results.

The simulation and experimental results show that the proposed method has the capability to diagnose the single and double IGBT modules open-circuit faults of GSC, and the accuracy is high.

Author Contributions: J.Z. and H.S. conceived the research direction. J.Z. designed the experiments, proposed TFA method and performed the simulation and experimental results analysis. J.Z. and Z.S. wrote the paper. Z.S., Y.D. and W.D. contributed to project research scheme formulation. All authors contributed to the final version.

Funding: This research was funded by the Hebei Education Department Fund (No. QN2016079), the Key Project of Hebei Natural Fund (No. E2018210044).

Acknowledgments: J.Z. thanks Prof. Haiyong Chen for his valuable advice. The authors thank all the reviewers and editors for their valuable comments and work.

Conflicts of Interest: The authors declare no conflict of interest.

References

1. Naderi, S.B.; Davari, P.; Zhou, D.; Negnevitsky, M; Blaabjerg, F. A review on fault current limiting devices to enhance the fault ride-through capability of the doubly-fed induction generator based wind turbine. *Appl. Sci.* **2018**, *8*, 2059.
2. Tian, J.; Zhou, D.; Su, C.; Blaabjerg, F.; Chen, Z. Optimal control to increase energy production of wind farm considering wake effect and lifetime estimation. *Appl. Sci.* **2017**, *7*, 65.
3. Lin, Y.G.; Tu, L.; Liu, H.W.; Li, W. Fault analysis of wind turbines in China. *Renewable & Sustainable Energy Reviews* **2016**, *55*, 482-490.
4. Shamshirband, S.; Rabczuk, T.; Chau, K.-W. A survey of deep learning techniques: application in wind and solar energy resources. *IEEE Access*, **2019**, *7*, 164650-164666.
5. Sun, Z.X.; Sun, H.X. Health status assessment for wind turbine with recurrent neural networks. *Mathmatical Problems in Engineering*, **2018**.
6. Cardoso, F.B.a.A.J.M. A comprehensive survey on fault diagnosis and fault tolerance of DC-DC converters. *Chinese Journal of Electrical Engineering*, **2018**, *4*.
7. Islam, F.R.; Prakash, K.; Mamun, K.A.; Lallu, A.; Pota, H.R. Aromatic network: a novel structure for power distribution system. *IEEE Access*, **2017**, *5*, 25236-25257.
8. Zhang, J.X.; Sun, H.X.; Sun, Z.X.; Dong, W.C.; Dong, Y. Fault diagnosis of wind turbine power converter considering wavelet transform, feature analysis, judgment and BP neural network. *IEEE Access* **2019**, *7*, 179799-179809.
9. Potamianos, P.G.; Mitronikas, E.D.; Safacas, A.D. Open-circuit fault diagnosis for matrix converter drives and remedial operation using carrier-based modulation methods. *IEEE Transactions on Industrial Electronics* **2014**, *61*, 531-545.

10. Gan, C.; Wu, J.H.; Yang, S.Y.; Hu, Y.H.; Cao, W.P.; Si, J.K. Fault diagnosis scheme for open-circuit faults in switched reluctance motor drives using fast Fourier transform algorithm with bus current detection. *IET Power Electronics* **2016**, *9*, 20-30.
11. Tian, L.S.; Wu, F.; Zhao, J. Current kernel density estimation based transistor open-circuit fault diagnosis in two-level three phase rectifier. *Electronics Letters* **2016**, *52*, 1795-U64.
12. Wang, K.; Tang, Y.; Zhang, C.J. Open-circuit fault diagnosis and tolerance strategy applied to four-wire T-type converter systems. *IEEE Transactions on Power Electronics* **2019**, *34*, 5764-5778.
13. Li, C.; Liu, Z.; Zhang, Y.; Chai, L.; Xu, B. Diagnosis and location of the open-circuit fault in modular multilevel converters: an improved machine learning method. *Neurocomputing* **2019**, *331*, 58-66.
14. Sobanski, P.; Kaminski, M. Application of artificial neural networks for transistor open-circuit fault diagnosis in three-phase rectifiers. *IET Power Electronics* **2019**, *12*, 2189-2200.
15. Zhao, H.S.; Cheng, L.L. Open-circuit faults diagnosis in back-to –back converters of DF wind turbine. *IET Renewable Power Generation* **2017**, *11*, 417-424.
16. Wang, M.; Zhao, J.; Wu, F.; Yang, H. Transistor open-circuit fault diagnosis of three phase voltage-source inverter fed induction motor based on information fusion. *2017 12th IEEE Conference on Industrial Electronics and Applications (ICIEA)*, **2017**, Siem Reap, Cambodia, 1591-1594.
17. Zheng, M.; Wen, H.; Shi, H.; Hu, Y.; Yang, Y.; Wang, Y. Open-circuit fault diagnosis of dual active bridge DC-DC converter with extended-phase-shift control. *IEEE Access* **2017**, *7*, 23752-23765.
18. Wind Power Capacity Worldwide Reaches 597 GW, 50,1 GW added in 2018 World Wind Energy Association. Accessed: Feb. 25, **2019**. [Online]. Available: https://wwindea.org/blog/2019/02/25/wind-power-capacity-worldwide-reaches-600-gw-539-gw-dded-in-2018/
19. Report on China's Wind Power Lifting Capacity in 2018 Chinese Wind Energy Association. Accessed: Apr. 5, **2019**. [Online]. Available: http://www.cwea.org.cn/news_lastest_detail.html?id=217
20. Yaramasu, V.; Dekka, A.; Duran, J.; Kouro, S.; Wu, B. PMSG-based wind energy conversion systems: survey on power converters and control. *IET Electric Power Applications* **2017**, *11*, 856-968.
21. Qiu, Y.; Jiang, H.; Feng, Y.; Cao, M.; Zhao, Y.; Li, D. A new fault diagnosis algorithm for PMSG wind turbine power converters under variable wind speed conditions. *Energies* **2016**, *9*, 548.
22. Dragomiretskiy, K.; Zosso, D. Variational mode decomposition. *IEEE Transactions on Signal Processing* **2014**, *62*, 531-544.
23. Isham, M.F.; Leong, M.S.; Lim, M.H.; Ahmad, Z.A. Variational mode decomposition: mode determination method for rotating machinery diagnosis. *Journal of Vibroengineering* **2018**, *20*, 2604-2621.
24. Dai, J.; Song, H.; Sheng, G.; Jiang, X. Cleaning method for status monitoring data of power equipment based on stacked denoising autoencoders. *IEEE Access* **2017**, *5*, 22863-22870.
25. Ma, M.; Sun, C.; Chen, X. Discriminative deep belief networks with ant colony optimization for health status assessment of machine. *IEEE Transactions on Instrumentation and Measurement* **2017**, *66*, 3115-3125.
26. Sun, Z.X.; Zhao, S.S.; Zhang, J.X. Term wind power forecasting on multiple scales using VMD decomposition, K-means clustering and LSTM principal computing. *IEEE Access* **2019**, *7*, 1266917-166929.